Maximal Convex Combinations of Sequential Steklov Eigenvalues

Weaam Alhejaili*and Chiu-Yen Kao[†]

February 2, 2019

Abstract

In this paper, we study a shape optimization problem in two dimensions where the objective function is the convex combination of two sequential Steklov eigenvalues of a domain with a fixed area constraint. We show the existence of the optimal domain and the nondecreasing, Lipschitz continuity, and convexity of the optimal objective function with respect to the convex combination constant. On one-parameter family of rectangular domains, asymptotic behaviors of lower eigenvalues are found. For general shapes, numerical approaches are used to find optimal shapes. The range of the first two Steklov eigenvalues are discussed for several one-parameter families of shapes including Cassini oval shapes and Hippopede shapes.

Keywords: Steklov eigenvalues, extremal eigenvalue problem, shape optimization, spectral method

AMS subject classifications. 35P15, 49Q10, 65N25

1 Introduction

Steklov eigenvalue problems have attracted many attentions lately due to their distinct properties from Dirichlet-Laplacian eigenvalue problems and their potential applications in wave problems. Steklov eigenvalue problems arise in the study of real physical phenomena. For examples, Steklov problems were used to model the vibrations of a vertical pendulum consisting of a bob suspended by a wire [1] and the oscillation of the fluid inside a container [27, 26, 30, 24, 8, 12].

Let $\Omega \subset \mathbb{R}^2$ be a bounded open set with Lipschitz boundary $\partial\Omega$, and (λ_k, u_k) denote the k-th eigenpair of the Steklov eigenvalue problem

$$\begin{cases} \Delta u(\mathbf{x}) = 0 & \text{in} \quad \Omega, \\ \frac{\partial u}{\partial n} = \lambda u & \text{on} \quad \partial \Omega, \end{cases}$$
 (1.1)

where \triangle is the Laplace operator and $\frac{\partial u}{\partial n} = \hat{\mathbf{n}} \cdot \nabla u$ is the directional derivative in the outward normal direction $\hat{\mathbf{n}}$. The Steklov problem (1.1) has a countable infinite set of eigenvalues which are greater than or equal to zero. We arrange them as $0 = \lambda_0(\Omega) < \lambda_1(\Omega) \le \lambda_2(\Omega) \le \cdots \le \lambda_k(\Omega) \le \cdots \to \infty$ and denote u_k as the corresponding eigenfunction in the Sobolev space $H^1(\Omega)$. The variational characterization of the eigenvalues is given by

$$\lambda_k(\Omega) = \min_{v \in H^1} \left\{ \frac{\int_{\Omega} |\nabla v|^2 dx}{\int_{\partial \Omega} v^2 ds} : \int_{\partial \Omega} v u_i = 0, \ i = 0, \dots, k - 1 \right\}.$$
 (1.2)

The eigenfunctions u_k are normalized so that

$$\int_{\partial\Omega} u_k^2 = 1. \tag{1.3}$$

^{*}E-mail: weaam.alhejaili@cgu.edu; Address: Institute of Mathematical Sciences, Claremont Graduate University, Claremont, CA 91711; E-mail:waalhejali@pnu.edu.sa; Address: Department of Mathematical Sciences, College of Sciences, Princess Nourah bint Abdulrahman University, Riyadh, Saudi Arabia.

[†]E-mail: ckao@cmc.edu; Address: Department of Mathematical Sciences, Claremont McKenna College, Claremont, CA 91711. This author's work is supported in part by a collaboration grant for mathematicians from Simons Foundation 514210 in 2017-2018 academic year and a NSF grant DMS-1818948.

Furthermore, Steklov eigenvalues satisfy the homothety property $\lambda_k(t\Omega) = t^{-1}\lambda_k(\Omega)$. This gives $\lambda_k(t\Omega)\sqrt{\mid t\Omega\mid} = \lambda_k(\Omega)\sqrt{\mid \Omega\mid}$. Instead of fixing the area $\mid \Omega\mid$, we consider the γ -parameterized shape optimization problem of maximizing the convex combination of sequential area-scaled Steklov eigenvalues,

$$J_{k,\gamma}(\Omega) =: \left\{ (1 - \gamma)\lambda_k^A(\Omega) + \gamma \lambda_{k+1}^A(\Omega) \right\} \quad \text{where} \quad \lambda_k^A(\Omega) = \lambda_k(\Omega)\sqrt{|\Omega|}$$
 (1.4)

for a given integer k and a given $\gamma \in [0, 1]$.

Here we review some shape optimization results of Steklov eigenvalues for different objective functions. In 1954, R. Weinstock [31] proved that

$$\lambda_1(\Omega) \le \frac{2\pi}{|\partial\Omega|} \tag{1.5}$$

where Ω is an open, bounded, and simply-connected domain in \mathbb{R}^2 . The equality in (1.5) holds if and only if Ω is a circle. Incorporating the classical isoperimetric inequality $|\partial\Omega|^2 \geq 4\pi |\Omega|$ leads to

$$\lambda_1^A(\Omega) = \lambda_1(\Omega)\sqrt{|\Omega|} \le \sqrt{\pi}.$$

For higher eigenvalues, Hersch, Payne, and Schiffer [23, Equation (3")] proved that

$$\sup\{\lambda_k(\Omega) \mid \partial\Omega \mid\} \le 2\pi k, \quad k \in \mathbb{N}.$$

This bound was proved to be sharp by Girouard and Polterovich [20] and it is attained by a sequence of simply connected domains degenerating into a disjoint union of k identical balls. In 2011, the isoperimetric inequality was generalized to arbitrary Riemannian surfaces by Fraser and Schoen [16].

The sum of squared reciprocal Steklov eigenvalues $\sum_{k=1}^{\infty} \lambda_k^{-2}$ for simply connected domains with a fixed perimeter is also minimized by a disk [15]. In [22], it was proved that the ball maximizes the product of the first n nonzero Steklov eigenvalues in \mathbb{R}^n . In 2015, Girouard, Laugesen, and Siudeja [19] found the sharp isoperimetric upper bound for the sum of the first k-th eigenvalues, partial sums of the spectral zeta function, and heat trace for star-like and simply-connected domains via the quasi-conformal mapping. In [11], Brock proved that, among domains of \mathbb{R}^n of prescribed volume, the ball maximizes the first Steklov eigenvalue.

All of these optimization results are achieved by identifying the optimal shape and proved that it is the desired optimizer. The existence of optimal domains that maximize general objective functions that depend on Steklov eigenvalues is studied in [10]. However, for most of shape optimization problems, even when the optimal shape exists, it cannot be identified explicitly in general. This motivates numerical approaches to find the optimal shapes.

Recently, Bogosel [9] used fundamental solutions to compute the Steklov, Wentzell, and Laplace-Beltrami eigenvalues and demonstrated that the ball is the maximizer for a variety of shape optimization problems. Akhmetgalyev, Kao, and Osting [3] considered the problems of maximizing λ_k^A among star-shaped domains via boundary integral methods. Alhejaili and Kao [5] proposed an efficient spectral method to find the Steklov eigenpairs and maximizes λ_k^A based on conformal mappings.

To the author's best knowledge, the convex combination of Steklov eigenvalues problem (1.4) has not been studied. When $\gamma=0$ or 1, it reduces to the maximization problem of Steklov eigenvalues studied in [9, 2, 5]. In the case of Dirichlet-Laplacian eigenvalues λ_k^D , the minimal convex combination was studied in [32, 28, 29, 25]. It was found that the range of the first two Dirichlet-Laplacian eigenvalues are bounded by two rays and a curve connecting their endpoints which were determined by studying the convex combination of the first two Dirichlet-Laplacian eigenvalues.

The aim of this paper is to study the convex combination of Steklov eigenvalues problem (1.4). Theoretically, we investigate the existence of optimal domain and the nondecreasing, Lipschitz continuity, and convexity of the optimal objective function with respect to the convex combination constant γ . To explain the properties of (1.4) clearly and concisely, we study the behaviors of lower eigenvalues on a one-parameter family of rectangular domains and corresponding shape optimization problems. For general star-shape domains, we use numerical approaches including boundary integral methods [3] and spectral methods based on conformal mappings [5] to find optimal shapes of (1.4) for k = 1 to 5. In addition, we explore numerically the range of the first two Steklov eigenvalues $(\lambda_1^A(\Omega), \lambda_2^A(\Omega))$ for several families of simply-connected domains including Cassini oval shapes and Hippopede shapes.

The rest of the paper is organized as follows. In section 2, we present some analytical properties of (1.4) and study Steklov eigenvalues on a one-parameter family of rectangular domains. In section 3, we study the shape optimization problem (1.4) for two sequential Steklov eigenvalues $\lambda_k^A, \lambda_{k+1}^A$ over a class of star-shaped domains numerically. In section 4, we explore numerically the range of the first two Steklov eigenvalues $(\lambda_1^A(\Omega), \lambda_2^A(\Omega))$ for several families of simply-connected domains. At the end, a brief discussion and possible future directions are given.

$\mathbf{2}$ Sequential Eigenvalues Problems

Here we first study several analytical properties of sequential Steklov eigenvalue problems on general domains and then discuss Steklov eigenvalues on rectangles in particular and their asymptotic properties. We show that, among all rectangular domains, the first area-scaled eigenvalue λ_1^A is maximized by a unit square and the limit of the ratio of first two eigenvalues is 4 when the aspect ratio of width and length goes to zero. The optimal rectangular shapes of (1.4) were found for k=1 to 5 for a given set of $\gamma \in [0,1]$.

Proposition 1. For the admissible set, $\mathcal{A} = \{\Omega \mid \Omega \subset \mathbb{R}^2 \text{, bounded and Lipschitz, has finite perimeter, and$ $|\Omega| = m$ where m is a given constant and the objective function (1.4), define

$$J_{k,\gamma}^* = \sup_{\Omega \in A} J_{k,\gamma}(\Omega) \quad and \quad \Omega_{k,\gamma}^* = \left\{ \Omega \in \mathcal{A} : J_{k,\gamma}(\Omega) = J_{k,\gamma}^* \right\}.$$

- 1. (Existence of the optimal domain). For given k and γ , this maximization problem has at least one solution $\Omega_{k,\gamma}^*$ which is given by the union of at most p disjoint Jordan domains whose closures intersect pairwise in at most one point. Moreover, every optimal set is bounded and contained in an optimal domain satisfying the aforementioned properties.
 - 2. The optimal value, $J_{k,\gamma}^*$, is a nondecreasing, Lipschitz continuous, and convex function of γ .

Proof. (1) This proof can be obtained by adapting the results in [10, Theorem 6.4] by checking the objective function

$$J_{k,\gamma}(\Omega) = m\left((1-\gamma)\lambda_k(\Omega) + \gamma\lambda_{k+1}(\Omega)\right)$$

which is not decreasing in λ_k and λ_{k+1} and upper semi-continuous for any given $\gamma \in [0,1]$.

(2) (a) Let $0 \leq \gamma_1 < \gamma_2 \leq 1$ and $\Omega_{\gamma_1} \in \Omega_{k,\gamma_1}^*$. Assume that $J_{k,\gamma_1}^* > J_{k,\gamma_2}^*$. Then $J_{k,\gamma_1}^* > J_{k,\gamma_2}^* \geq J_{k,\gamma_2}(\Omega_{\gamma_1}) \geq J_{k,\gamma_1}(\Omega_{\gamma_1})$ since $J_{k,\gamma}$ is nondecreasing in γ . However, this contradicts that $\Omega_{\gamma_1} \in \Omega_{k,\gamma_1}^*$. Thus $J_{k,\gamma}^*$ is nondecreasing in γ .

(b) Assume $\Omega_1 \in \Omega_{k,\gamma_1}^*$ and $\Omega_2 \in \Omega_{k,\gamma_2}^*$, respectively. Since

$$\begin{split} J_{k,\gamma_{2}}^{*} - J_{k,\gamma_{1}}^{*} &= J_{k,\gamma_{2}}(\Omega_{2}) - J_{k,\gamma_{1}}(\Omega_{1}) \\ &= J_{k,\gamma_{2}}(\Omega_{2}) - J_{k,\gamma_{1}}(\Omega_{2}) + J_{k,\gamma_{1}}(\Omega_{2}) - J_{k,\gamma_{1}}(\Omega_{1}) \\ &\leq J_{k,\gamma_{2}}(\Omega_{2}) - J_{k,\gamma_{1}}(\Omega_{2}) \\ &= (\gamma_{2} - \gamma_{1}) \left(\lambda_{k+1}^{A}(\Omega_{2}) - \lambda_{k}^{A}(\Omega_{2}) \right) \end{split}$$

which shows that $J_{k,\gamma}^*$ is Lipschitz continuous with Lipschitz constant $\lambda_{k+1}^A(\Omega_2) - \lambda_k^A(\Omega_2)$. (c) The proof of convexity is done by contradiction. Let $\gamma_\alpha = (1-\alpha)\gamma_1 + \alpha\gamma_2$ for $\alpha \in (0,1)$ and note that for any Ω ,

$$J_{k,\gamma_{\alpha}}(\Omega) = (1 - \alpha) J_{k,\gamma_{1}}(\Omega) + \alpha J_{k,\gamma_{2}}(\Omega).$$

Let $\Omega_{\alpha} \in \Omega_{k,\gamma_{\alpha}}^*$ and suppose that

$$J_{k,\gamma_{\alpha}}^* > (1-\alpha) J_{k,\gamma_1}^* + \alpha J_{k,\gamma_2}^*.$$

Then

$$\begin{split} J_{k,\gamma_2}(\Omega_\alpha) &= \frac{1}{\alpha} J_{k,\gamma_\alpha}(\Omega_\alpha) - \frac{(1-\alpha)}{\alpha} J_{k,\gamma_1}(\Omega_\alpha) \\ &\geq \frac{1}{\alpha} J_{k,\gamma_\alpha}(\Omega_\alpha) - \frac{(1-\alpha)}{\alpha} J_{k,\gamma_1}^* \\ &> \frac{1-\alpha}{\alpha} J_{k,\gamma_1}^*(\Omega) + J_{k,\gamma_2}^* - \frac{(1-\alpha)}{\alpha} J_{k,\gamma_1}^*(\Omega) \\ &= J_{k,\gamma_2}^* \end{split}$$

which contradicts the optimality of J_{k,γ_2}^* . This shows that J_{k,γ_2}^* is a convex function of γ .

2.1 Steklov Eigenvalues and Eigenfunctions on Rectangular Domains

Consider a class of one parameter rectangular domains $R_a := (-1,1) \times (-a,a) \subset \mathbb{R}^2$. The aspect ratio of the rectangle is $a \in (0,1]$ and the area of the rectangle is given by $|R_a| = 4a$. As discussed in [6] by using the method of separation of variables, Steklov eigenpairs (λ_k, u_k) of (1.1) on R_a can be found and summarized in eight difference cases which are listed in Table 1. Steklov eigenvalues and eigenfunctions are arranged according to the symmetry of eigenfunctions with respect to variables x and y. In Table 1, eigenfunctions are listed in the second column, eigenvalues are listed in the fourth column in which each $\nu > 0$ has to satisfy the corresponding condition listed in the third column. The last column indicates the corresponding eigenvalue curve colors and styles in Figure 2.4(A). It is interesting to see that, when $a \to 0$, IV(2) (blue solid curves) give odd eigenvalues while I(2) (red solid curves) give even eigenvalues. When $a \to 1$, eigenvalues of I(2) (red solid curves) and III(2) (green solid curves) are asymptotically close to each other. In addition, eigenvalues of IV(2) (blue solid curves) and III(2) (black solid curves) are asymptotically close to each other for odd $k \ge 3$. In Figure 2.1, we show the first ten eigenfunctions for $R_{0,2}$.

Class	Eigenfunctions u_k	Condition on ν	Eigenvalues λ_k	Curves in Figure 2.4(A)
I(1)	$\cosh(\nu x)\cos(\nu y)$	$\tan(a\nu) = -\tanh(\nu)$	$\nu \tanh(\nu)$	red dash
I(2)	$\cos(\nu x)\cosh(\nu y)$	$\tan(\nu) = -\tanh(a\nu)$	$\nu \tanh(a\nu)$	red solid
II(1)	$\sinh(\nu x)\sin(\nu y)$	$\tan(a\nu) = \tanh(\nu)$	$\nu \coth(\nu)$	black dash
II(2)	$\sin(\nu x)\sinh(\nu y)$	$\tan(\nu) = \tanh(a\nu)$	$\nu \coth(a\nu)$	black solid
III(1)	$\cosh(\nu x)\sin(\nu y)$	$\tan(a\nu) = \coth(\nu)$	$\nu \tanh(\nu)$	green dash
III(2)	$\cos(\nu x)\sinh(\nu y)$	$\tan(\nu) = -\coth(a\nu)$	$\nu \coth(a\nu)$	green solid
IV(1)	$\sinh(\nu x)\cos(\nu y)$	$\tan(a\nu) = -\coth(\nu)$	$\nu \coth(\nu)$	blue dash
IV(2)	$\sin(\nu x)\cosh(\nu y)$	$\tan(\nu) = \coth(a\nu)$	$\nu \tanh(a\nu)$	blue solid

Table 1: The eigenfunctions and eigenvalues on rectangles R_a .

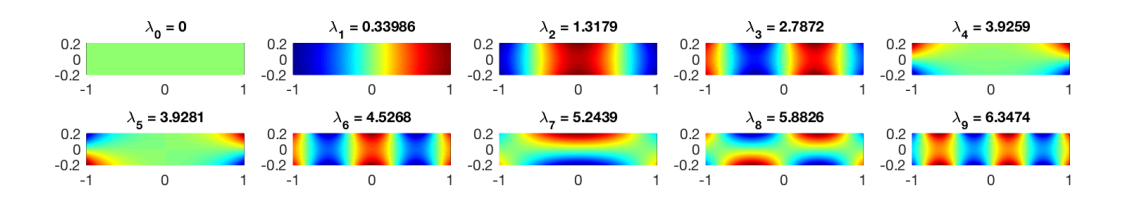


Figure 2.1: The first ten eigenvalues and their corresponding eigenfunctions on the rectangle $R_{0.2}$.

When a = 1, R_a is a square. Due to symmetry, the aforementioned eight cases can be reduced to four cases as discussed in [17]. The results are summarized in Table 2 and the first ten eigenvalues and

eigenfunctions are shown in Figure 2.2. In this case, there is an additional eigenfunction xy corresponding to the eigenvalue 1.

Eigenfunctions u_k	Condition on ν	Eigenvalues λ_k
xy		1
$\frac{\cosh(\nu x)\cos(\nu y)}{\cos(\nu x)\cosh(\nu y)}$	$\tan(\nu) = -\tanh(\nu)$	$ u \mathrm{tanh}(u)$
$\frac{\sinh(\nu x)\sin(\nu y)}{\sin(\nu x)\sinh(\nu y)}$	$\tan(\nu) = \tanh(\nu)$	$\nu \mathrm{coth}(\nu)$
$\frac{\cosh(\nu x)\sin(\nu y)}{\sin(\nu x)\cosh(\nu y)}$	$\tan(\nu) = \coth(\nu)$	$ u \tanh(\nu) $
$\frac{\cos(\nu x)\sinh(\nu y)}{\sinh(\nu x)\cos(\nu y)}$	$\tan(\nu) = -\coth(\nu)$	$ u \coth(u) $

Table 2: The eigenfunctions and eigenvalues on the square R_1 .

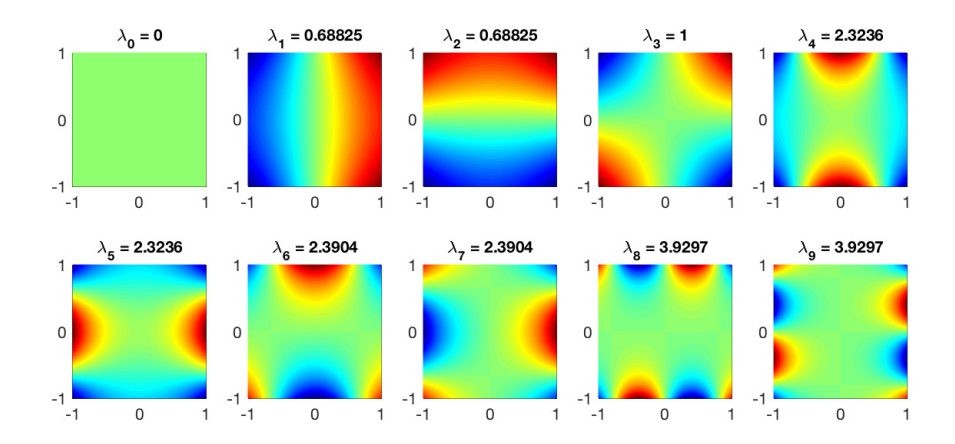


Figure 2.2: The first ten eigenvalues and their corresponding eigenfunctions on the square R_1 .

Lemma 2. The first eigenvalue λ_1^A of rectangle R_a , $a \in (0,1]$ is determined by case IV(2) in Table 1.

Proof. To explain the idea clearly, in Figure 2.3, we plot the functions that are used to determine the conditions on ν in Table 1 for a=0.1. It is observed that the first intersection $\nu_1>0$ of two curves happens when IV(2) $\tan(\nu_1)=\coth(a\nu_1)$ is satisfied for $\nu_1\in(0,\pi/2)$. This is true because, for a sufficiently small ϵ , there is a unique $\nu_1\in[\epsilon,\frac{\pi}{2}-\epsilon]$ such that $\tan(\nu_1)=\coth(a\nu_1)$ due to the Intermediate Value Theorem and monotonicity. Furthermore, it is observed the rest of intersection happens at $\nu>\nu_1$. Since $\tanh(a\nu)\leq \tanh(\nu)<1<\coth(a\nu)\leq \coth(\nu)$ for all ν and $a\in(0,1]$, this implies that

$$\nu \tanh (a\nu) \le \nu \tanh (\nu) < \nu < \nu \coth(a\nu) \le \nu \coth(\nu)$$

for all ν and $a \in (0, 1]$. This ordering property tells us that the first eigenvalue λ_1 is determined by IV(2) so does the first area-scaled eigenvalue λ_1^A . To show that the rest of intersection happens at $\nu > \nu_1$, we discuss each case. For cases I(1), I(2), III(2), and IV(1), there is no intersection on $(0, \pi/2)$ due to the positivity of $\tan(\nu)$ and $\tan(a\nu)$ and negativity of $-\coth(\nu)$ and $-\coth(a\nu)$. For case II(2), there is no intersection on $(0, \pi/2)$ because $\tan(\nu) - \tanh(a\nu)$ is a monotone increasing function. For case III(1), the intersection

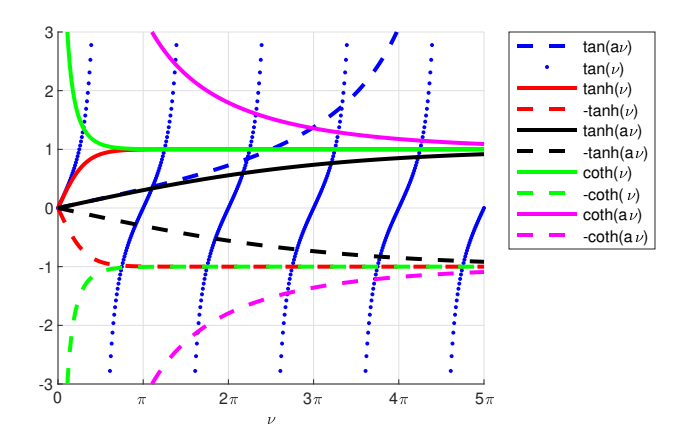


Figure 2.3: The conditions on ν as defined in Table 1 for a=0.1.

of $\tan(a\nu)$ and $\coth(\nu)$ is monotone decreasing in a. When $a=1, \nu=\nu_1$. Thus if $a<1, \nu>\nu_1$. For case II(1), the intersection of $\tan(a\nu)$ and $\tanh(\nu)$ is monotone decreasing in a too. Furthermore, there is no intersection when a=1 and $\nu<\frac{\pi}{2}$. In this case, the intersection must only occur when $\nu>\nu_1$. This concludes the proof.

Lemma 3. The first non-zero area-scaled eigenvalue λ_1^A of R_a is a monotone increasing function on the interval (0,1]. The square R_1 maximizes the first Steklov eigenvalue λ_1^A among all rectangular shapes R_a where $a \in (0,1]$.

Proof. From Lemma 2, we know that, for a sufficiently small ϵ , there is a unique $\nu \in [\epsilon, \frac{\pi}{2} - \epsilon]$ such that $\tan(\nu) = \coth(a\nu)$ due to the Intermediate Value Theorem and monotonicity. The determining condition of ν can be rewritten as $\nu \tanh(a\nu) - \nu \coth(\nu) = 0$ which can be easily linked to the first non-zero eigenvalue $\lambda_1 = \nu \tanh(a\nu)$.

Let $1 \ge a_1 > a_2 > 0$ and define $D(a, \nu) = \nu \tanh(a\nu) - \nu \cot(\nu)$. Denote ν_1 and $\nu_2 \in (0, \pi/2)$ are roots of $D(a, \nu) = 0$ for different a_1 and a_2 . Thus, $D(a_1, \nu_1) = 0$ and $D(a_2, \nu_2) = 0$. It is clear that D is a monotone increasing function of a when ν is fixed. Similarly, D is a monotone increasing function of ν when a is fixed. Since $a_1 > a_2$, and $D(a_1, \nu_1) = 0$, this implies that $D(a_2, \nu_1) < 0$. Furthermore, $D(a_2, \nu_2) = 0$, thus $\nu_1 < \nu_2$. Since $\lambda_1 = \nu \tanh(a\nu) = \nu \cot(\nu)$ and $\nu \cot(\nu)$ is a monotone decreasing function, we have $\lambda_1(\nu_1) > \lambda_1(\nu_2)$. Thus, $\lambda_1(a)$ is a monotone increasing function on the interval (0,1] so is λ_1^A as the square root of the area $\sqrt{4a}$ is also an increasing function of a.

Inspired by this lemma, we conjecture that n-cube is the maximizer among n-orthotope (hyperrectangles) in \mathbb{R}^n . Note that Brock [11] proved that, among domains of \mathbb{R}^n of prescribed volume, the ball maximizes the first Steklov eigenvalue.

2.2 Asymptotic Behavior of λ_k^A for Rectangles

Based on Figure 2.4(A), we notice that when a is small enough, the lower eigenvalues are determined by either case IV(2) (blue solid curves) or case I(2) (red solid curves) and these eigenvalues approach to zero when $a \to 0$. For the eigenvalues which are determined by other cases, the values seem divergent. In the following, we explore asymptotic properties of eigenvalues in cases IV(2) and I(2).

Lemma 4. For any given $k \in \mathbb{N}^+$, the eigenvalues λ_k^A of rectangular shapes R_a satisfy the following asymptotic expansion

$$\lambda_k^A = \frac{k^2 a^{\frac{3}{2}} \pi^2}{2} + O(a^{\frac{5}{2}}), \quad a \to 0.$$

Proof. We discuss odd eigenvalues determined by case IV(2) and even eigenvalues determined by case I(2), respectively. For case IV(2) in Table 1, the determining condition $tan(\nu) = coth(a\nu)$ is equivalent to

$$\tanh(a\nu) = \cot(\nu). \tag{2.1}$$

When a is small, the first zero $\nu_1 > 0$ will be close to $\frac{\pi}{2}$ due to monotonicity of $\cot(\nu)$ and $\cot(\frac{\pi}{2}) = 0$. Due to the periodicity of $\cot(\nu)$, the rest of roots ν_n will be close to $\frac{(2n-1)\pi}{2}$. The $\nu_n \tan(a\nu_n)$ gives λ_{2n-1} eigenvalues.

Denote $y_b = \frac{b\pi}{2} - \nu_n$ with b = 2n - 1 and compute the Taylor expansion of (2.1) near $y_b = 0$ and a = 0. The second order expansion leads to a linear equation for y_b

$$(1+a)y_b - \frac{ab\pi}{2} = 0$$

which gives

$$y_b = \frac{ab\pi}{2(1+a)}.$$

Since $\lambda_{2n-1}^A = \sqrt{4a} \nu_n \tanh(a\nu_n) \approx 2a^{\frac{3}{2}} \nu_n^2$, we obtain

$$\lambda_{2n-1}^A \approx 2a^{\frac{3}{2}} \left(\frac{b\pi}{2} - \frac{ab\pi}{2(1+a)}\right)^2 \approx \frac{a^{\frac{3}{2}}b^2\pi^2(1-2a)}{2}$$

in which we use $\frac{1}{1+a} \approx 1 - a$ as $a \to 0$. This gives

$$\lambda_{2n-1}^A = \frac{(2n-1)^2 a^{\frac{3}{2}} \pi^2}{2} + O(a^{\frac{5}{2}}), \quad a \to 0.$$

For case I(2) in Table 1, the determining condition is

$$\tan(\nu) + \tanh(a\nu) = 0. \tag{2.2}$$

When a is very small, the roots ν_n are close to $n\pi$ and $\nu_n \tanh(a\nu_n)$ gives λ_{2n} eigenvalues. Denote $y_c = c\pi - \nu_n$ with $c = n \in \mathbb{N}^+$ and compute the Taylor expansion of (2.2) near $y_c = 0$ and a = 0. The second order expansion leads to a linear equation of y_c

$$(1+a)y_c - ac\pi = 0$$

which gives

$$y_b = \frac{ac\pi}{1+a}.$$

Since $\lambda_{2n}^A = \sqrt{4a} \nu_n \tanh(a\nu_n) \approx 2a^{\frac{3}{2}} \nu_n^2$, we obtain

$$\lambda_{2n}^A \approx 2a^{\frac{3}{2}} \left(c\pi - \frac{ac\pi}{1+a} \right)^2 \approx 2a^{\frac{3}{2}} c^2 \pi^2 (1-2a)$$

in which we use $\frac{1}{1+a} \approx 1 - a$ as $a \to 0$. This gives

$$\lambda_{2n}^{A} = \frac{(2n)^2 a^{\frac{3}{2}} \pi^2}{2} + O(a^{\frac{5}{2}}), \quad a \to 0.$$
 (2.3)

In summary, for any given $k \in \mathbb{N}^+$, the eigenvalues λ_k^A of rectangular shapes R_a satisfy the following asymptotic expansion

$$\lambda_k^A = \frac{k^2 a^{\frac{3}{2}} \pi^2}{2} + O(a^{\frac{5}{2}}), \quad a \to 0.$$

Lemma 5. The ratio of the first and second Steklov eigenvalues satisfies the following asymptotic expansion

$$\lim_{a \to 0} \frac{\lambda_2^A}{\lambda_1^A} = 4.$$

Proof. This result follows immediately as

$$\lim_{a \to 0} \frac{\lambda_2^A}{\lambda_1^A} = \frac{\frac{2^2 \pi^2 a^{3/2}}{2}}{\frac{1^2 \pi^2 a^{3/2}}{2}} = 4.$$

2.3 Combination of Sequential Eigenvalues on Rectangles

In this section we study the γ -parameterized shape optimization problem of maximizing the convex combination of two sequential Steklov eigenvalues in the class of one parameter rectangular domains R_a . Based on Table 1, eigenvalues λ_k for rectangles R_a with different values of a can be determined by a root finding algorithm. In Figure 2.4(A) the area-scaled eigenvalues $\lambda_k^A(R_a) = \lambda_k(R_a)\sqrt{4a}$ are plotted for different values of a. The curve colors and styles that are listed in Table 1 are used to visualize the behavior of eigenvalues with respect to $a \in (0,1]$. It is interesting to see that, when a is small enough, the lower odd eigenvalues are determined by case IV(2) indicated by blue solid curves while the lower even eigenvalues are determined by case I(2) indicated by red solid curves. We verify numerically that these eigenvalues follow the asymptotic expressions which were proved in Lemma 4.

In Figure 2.4(B), the range of λ_k^A is taken to be smaller than 2.4(A) in order to show clearly the lower eigenvalues λ_k^A , $k=1,\ldots,6$. We recolor the curves in Figure 2.4(B) and labeled each λ_k^A on top of each curve. It is observed numerically that λ_1^A is a monotone increasing function which was proved in Lemma 3.

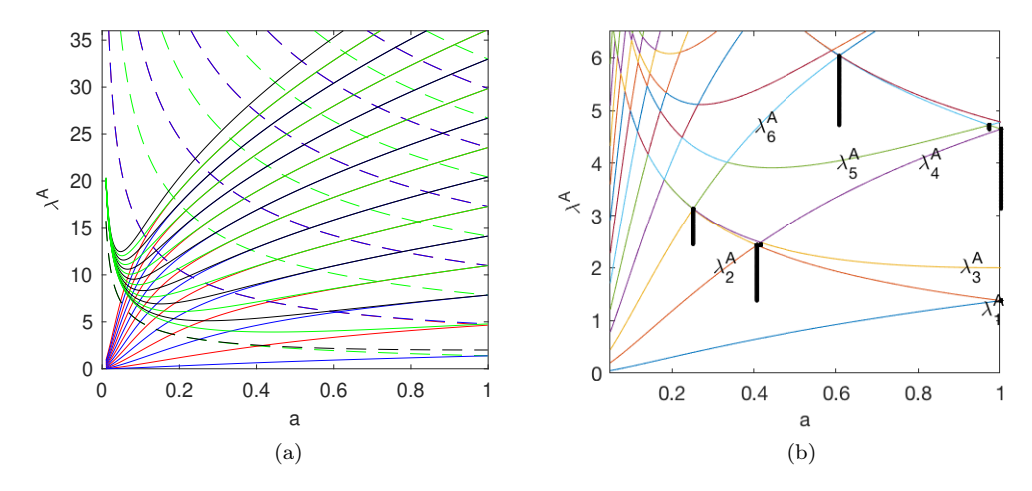


Figure 2.4: (A) Eigenvalues λ_k^A for rectangular domains R_a with $a \in (0,1]$ as defined in Table 1. (B) The lower eigenvalues λ_k^A . The black lines indicate the optimal values $\left(a, J_{k,\gamma}^* (R_a)\right)$ for $k = 1, \ldots, 5$, and $\gamma \in [0,1]$.

Now for a given $\gamma \in [0,1]$, we maximize the convex combination of two sequential Steklov eigenvalues λ_k and λ_{k+1} over a class of a-parameter rectangles. In Table 3, the optimal values $J_{k,\gamma}^*$ and the optimal aspect ratios a are summarized. In Figure 2.4(B), black lines indicate optimal values $\left(a, J_{k,\gamma}^* (R_a)\right)$ for $k = 1, \ldots, 5$. In Figure 2.5(A-E), we plot optimal values $J_{k,\gamma}^*, k = 1, \ldots, 5$ with respect to different values of $\gamma \in [0,1]$

and their corresponding optimal rectangles. It is observed that a square is sometimes, but not alway, the optimal rectangle. The red rectangles and red dots are used to highlight multiple optimal rectangles R_a^* which achieve the same optimal value $J_{k,\gamma}^*$ for the specific γ .

γ	$J_{1,\gamma}^*$	a	$J_{2,\gamma}^*$	a	$J_{3,\gamma}^*$	a	$J_{4,\gamma}^*$	a	$J_{5,\gamma}^*$	a
0	1.3765	1	2.4297	0.4063	3.1291	0.2513	4.6473	1	4.7225	0.9718
0.1	1.3765	1	2.4297	0.4063	3.1292	0.2513	4.6473	1	4.7225	0.9718
0.2	1.3765	1	2.4297	0.4063	3.1293	0.2513	4.6473	1	4.7226	0.9717
0.3	1.3765	1	2.4297	0.4063	3.1294	0.2513	4.6473	1	4.7226	0.9717
0.4	1.3765	1	2.4314	0.4158	3.1301	0.2517	4.6473	1	4.8435	0.6084
0.5	1.5384	0.4063	2.4396	0.4158	3.3236	0.2517	4.6474	0.9718	5.0425	0.6084
0.6	1.7166	0.4063	2.4833	0.2513	3.5884	1	4.6623	0.9718	5.2415	0.6084
0.7	1.8949	0.4063	2.6448	0.2513	3.8531	1	4.6773	0.9718	5.4404	0.6084
0.8	2.0732	0.4063	2.8062	0.2513	4.1178	1	4.6922	0.9718	5.6394	0.6084
0.9	2.2514	0.4063	2.9677	0.2513	4.3825	1	4.7071	0.9718	5.8384	0.6084
1	2.4297	0.4063	3.1291	0.2513	4.6473	1	4.7220	0.9718	6.0374	0.6084

Table 3: The optimal values $J_{k,\gamma}^*$ and the maximizers R_a^* for $k=1,\ldots,5$ and $\gamma\in[0,1].$

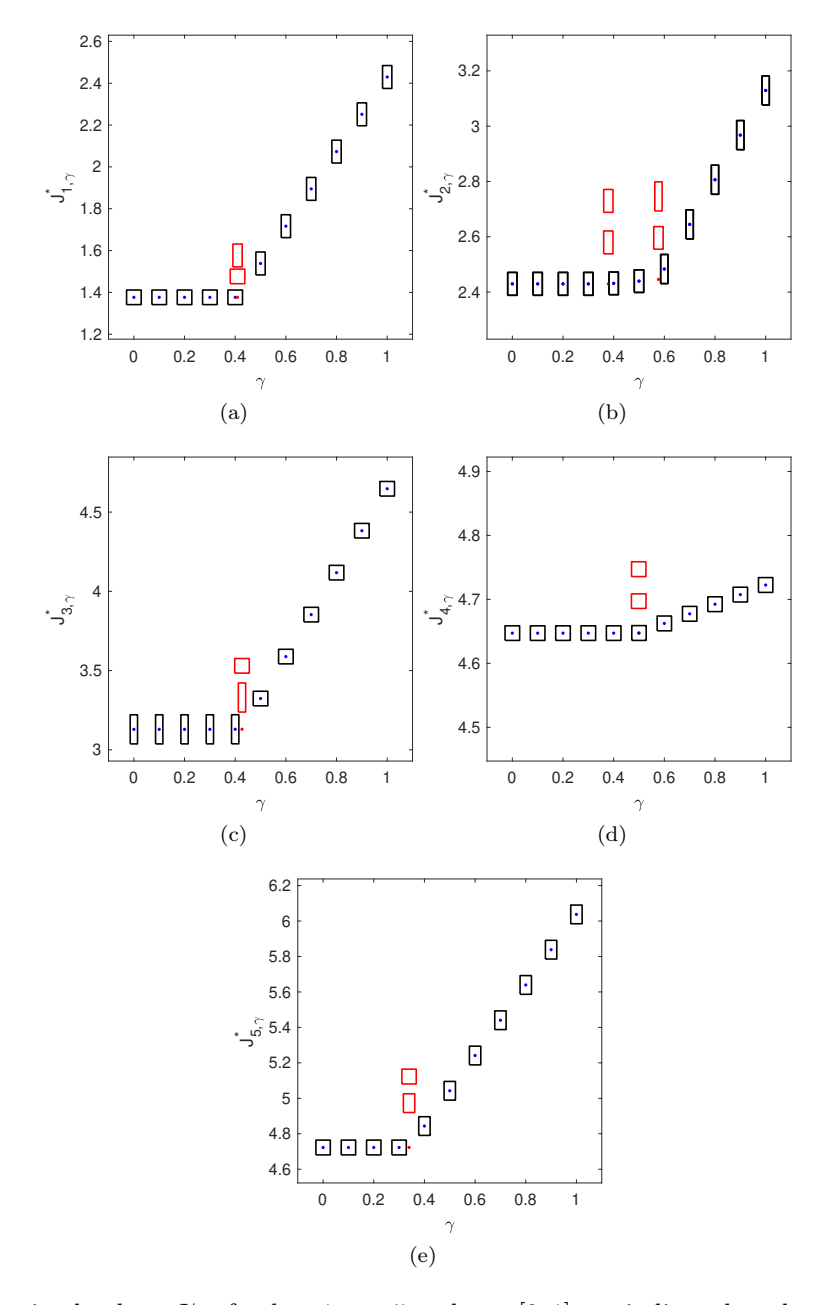


Figure 2.5: The optimal values $J_{k,\gamma}^*$ for $k=1,\ldots,5$ and $\gamma\in[0,1]$ are indicated as dots in the figures. For each dot, its corresponding optimal rectangle R_a^* is shown. The red rectangles and red dots are used to highlight multiple optimal rectangles R_a^* which achieve the same optimal value $J_{k,\gamma}^*$ for the specific γ .

2.3.1 Numerical Results and Observations

From Table 3 and Figure 2.5(A-E), we obtain the following conclusions. The optimal value, $J_{k,\gamma}^*$, $k=1,\ldots,5$ exists and is a nondecreasing, Lipschitz continuous, and convex function of γ as discussed in Proposition 1. The optimal rectangle R_a^* may not be unique. In Table 4, the values of γ are reported when several different optimal rectangles R_a^* exist and give the same optimal value $J_{k,\gamma}^*$. For $k=1,\ldots,5$, it is observed that the optimal value, $J_{k,\gamma}^*$ is a constant function in the beginning of the interval $\gamma \in [0,1]$.

k	γ	$J_{\gamma,k}^*$	a
1	0.4092	1.3765	0.4063 & 1
2(i)	0.3789	2.4297	0.4063 & 0.4158
2(ii)	0.5768	2.4459	0.2513 & 0.4158
3	0.4268	3.1301	0.2517 & 1
4	0.4989	4.6473	0.9718 & 1
5	0.3393	4.7225	0.6084 & 0.9718

Table 4: The optimal values $(\gamma, J_{k,\gamma}^*)$, k = 1, ..., 5 which are shown as red dotes in Figures 2.5 and their corresponding optimal rectangles with different aspect ratios of a.

3 Shape Optimization Approach

In this section we study the shape optimization problem (1.4) for two sequential Steklov eigenvalues λ_k, λ_{k+1} over a class of star-shaped domain Ω_n . We solve the forward problem by finding the eigenpair (λ_k, u_k) of (1.1) using boundary integral methods [2, 13] for a given domain. To evolve a domain to the optimal shape, we apply gradient-based optimization methods that require to compute the sensitivity of the objective function with respect to the variation of parameters which are used to present the star-shaped domains.

We choose boundary integral methods due to their computational efficiency and spectral accuracy. Unlike finite element methods [21, 7, 9] which require to discretize a given domain, boundary integral methods only discretize the boundary of the domain. Furthermore, the optimization problems require changing of domains which results in moving meshes in finite element approaches or incorporating other techniques to handle moving domains.

3.1 Numerical Approaches

We consider a class of star-shaped domains which are parametrized as

$$\Omega = \{(r,\theta) : 0 \le r \leqslant \rho_n(\theta), \theta \in [0,2\pi]\}, \quad \text{where} \quad \rho_n(\theta) = a_0 + \sum_{j=1}^n a_j \cos(j\theta) + b_j \sin(j\theta). \tag{3.1}$$

Thus the initial shape that we choose depends on coefficients a_0 , a_j , and b_j for $j \ge 1$. Given these coefficients, we use boundary integral methods [13, 2, 3] to find Steklov eigenvalues and eigenfunctions. Instead of discretizing the equation directly, boundary integral methods for solving Steklov problems represent an eigenfunction $u(\mathbf{x})$ based on a modified single layer potential and rewrite (1.1) into an integral eigenvalue equation. The numerical quadrature rules which can provide spectrally accuracy are used to take care of logarithmic singularity in the integral. See [13, 2, 3] for more details.

To find the optimal coefficients which represent the optimal domain, we first find the derivatives of $J_{k,\gamma}$ with respect to coefficients and then apply gradient-based optimization methods to minimize $J_{k,r}$ by using the optimization approach discussed in [3]. These derivatives are given in the following proposition.

Proposition 6. The derivatives of $J_{k,\gamma}$ with respect to Fourier coefficients are

$$\frac{\partial J_{k,\gamma}}{\partial a_j} = (1 - \gamma) \frac{\partial \lambda_k^A(\Omega)}{\partial a_j} + \gamma \frac{\partial \lambda_{k+1}^A(\Omega)}{\partial a_j},$$
$$\frac{\partial J_{k,\gamma}}{\partial b_i} = (1 - \gamma) \frac{\partial \lambda_k^A(\Omega)}{\partial b_i} + \gamma \frac{\partial \lambda_{k+1}^A(\Omega)}{\partial b_i},$$

where

$$\begin{split} \frac{\partial \lambda_k^A(\Omega)}{\partial a_j} &= \sqrt{|\Omega|} \int_0^{2\pi} \left(\left(|\nabla u_k|^2 - 2\lambda_k^2 u_k^2 - \lambda_k \kappa u_k^2 \right) + \lambda_k(\Omega) \frac{1}{2|\Omega|} \right) \rho(\theta) \cos(j\theta) d\theta, \\ \frac{\partial \lambda_k^A(\Omega)}{\partial b_j} &= \sqrt{|\Omega|} \int_0^{2\pi} \left(\left(|\nabla u_k|^2 - 2\lambda_k^2 u_k^2 - \lambda_k \kappa u_k^2 \right) + \lambda_k(\Omega) \frac{1}{2|\Omega|} \right) \rho(\theta) \sin(j\theta) d\theta. \end{split}$$

Proof. Consider the perturbation $\mathbf{x} \mapsto \mathbf{x} + t\mathbf{V}$ where \mathbf{V} is a vector field in the Sobolev space $W^{3,\infty}(\Omega,\mathbb{R}^2)$ and denote $V_n = \mathbf{V} \cdot \hat{\mathbf{n}}$ where $\hat{\mathbf{n}}$ is the outward unit normal vector. Assume that λ_k and λ_{k+1} are simple, based on the formula of shape derivative of λ_k^A given in [14, 3, 5, 4] and the addition rule of derivatives, the shape derivative of the combination of area-scaled sequential Steklov eigenvalues satisfies

$$J'_{k,\gamma}(\Omega) = (1 - \gamma) \left(\lambda_k^A(\Omega)\right)' + \gamma \left(\lambda_{k+1}^A(\Omega)\right)'$$

where ' denotes the shape derivative and

$$\left(\lambda_k^A(\Omega)\right)' = \sqrt{|\Omega|} \int_{\partial\Omega} \left(\left(|\nabla u_k|^2 - 2\lambda_k^2 u_k^2 - \lambda_k \kappa u_k^2 \right) + \lambda_k(\Omega) \frac{1}{2|\Omega|} \right) V_n ds$$

where κ is the curvature of $\partial\Omega$ and u_k is the corresponding normalized eigenfunction satisfying the normalization condition (1.3). Since the velocities **V** corresponding to a perturbation of the j-th cosine and sine coefficients are given by

$$\frac{\partial \mathbf{x}(\theta)}{\partial a_j} \cdot \hat{\mathbf{n}} = \frac{\rho(\theta)\cos(j\theta)}{\sqrt{\rho^2(\theta) + (\rho'(\theta))^2}}, \quad \frac{\partial \mathbf{x}(\theta)}{\partial b_j} \cdot \hat{\mathbf{n}} = \frac{\rho(\theta)\sin(j\theta)}{\sqrt{\rho^2(\theta) + (\rho'(\theta))^2}},$$

the proposition is proved by using the chain rule and changing the integral in the polar coordinates along boundary $\partial\Omega$.

3.2 Numerical Results and Observation

In this section, we apply aforementioned computational methods to study the convex combination of sequential Steklov eigenvalues problem (1.4) among general star-shaped domains. We parametrize the boundary with N=256 points with a uniform grid in θ direction. In our calculation, we use 61 modes, i.e. ρ_{30} with $a_0,\ a_j$ and $b_j,j=1,\ldots,30$. We initialize the shape with parameters $a_0=2.5,\ a_{k+1}=0.5$ and perturb all coefficients by small random numbers to generate initial random shapes. The optimal values, $J_{k,\gamma}^*$, for $k=1,\ldots,5$ are listed in Table 5 and the corresponding optimal shapes are shown in Figures 3.1, 3.2 and 3.3. From these results, we confirm that the function $J_{k,\gamma}^*$ is a nondecreasing, Lipschitz continuous, and convex function of γ as discussed in Proposition 1. For $k=1,\ldots,5$, it is observed that the optimal value, $J_{k,\gamma}^*$ is a constant function in the beginning of the interval $\gamma \in [0,1]$. When $\gamma=0$ or 1, we obtain optimal domains for maximizing k—th eigenvalues that were presented in [9, 3, 5]. When k=1, the optimal shape $\Omega_{1,\gamma}^*$ is a circle for a small enough γ and a two-fold symmetric shape for a large enough γ . When k=4, the optimal shape $\Omega_{4,\gamma}^*$ has either 4-fold or 5-fold symmetry. For k=2,3, and 5, there is a transition from k-fold symmetry to (k+1)-fold symmetry on the optimal domains.

$\gamma \setminus k$	1	2	3	4	5
0	1.7725	2.9161	4.1453	5.2844	6.4964
0.1	1.7725	2.9161	4.1453	5.2844	6.4964
0.2	1.7725	2.9161	4.1453	5.2844	6.4964
0.3	1.7725	2.9161	4.1453	5.285	6.4964
0.4	1.7725	2.9161	4.1453	5.3073	6.4964
0.5	1.8775	2.9573	4.1453	5.3298	6.4964
0.6	2.0782	3.0185	4.1453	5.326	6.4964
0.7	2.2834	3.2412	4.2372	5.3755	6.5016
0.8	2.4919	3.5384	4.5552	5.599	6.6271
0.9	2.703	3.8402	4.9184	6.0439	7.1244
1	2.9161	4.1453	5.2844	6.4964	7.644

Table 5: The optimal values $J_{k,\gamma}^*$ for $k=1,\ldots,5$ and $\gamma\in[0,1]$ for maximizing (1.4).

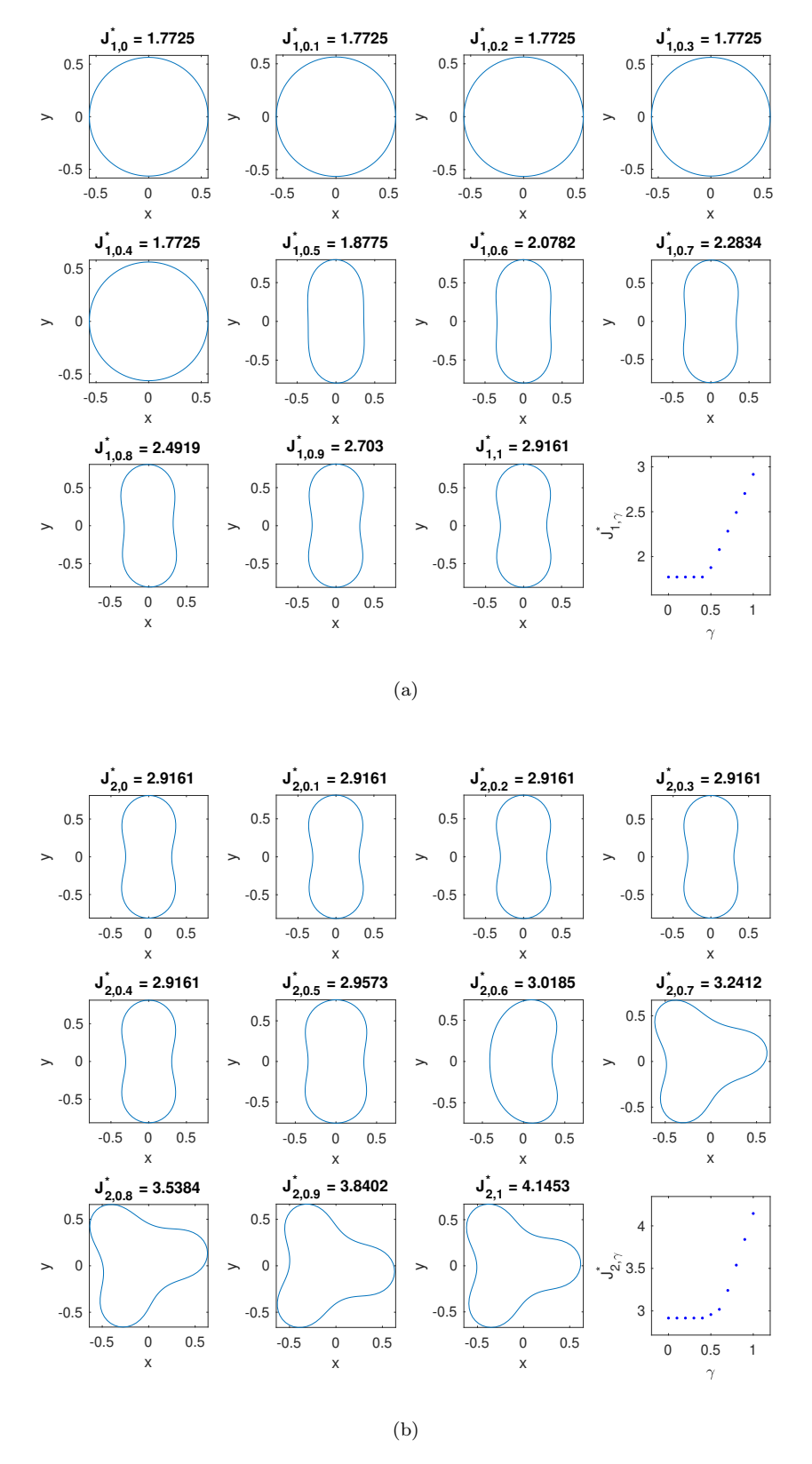


Figure 3.1: $J_{k,\gamma}^*$ for k=1,2 and $\gamma\in[0,1].$

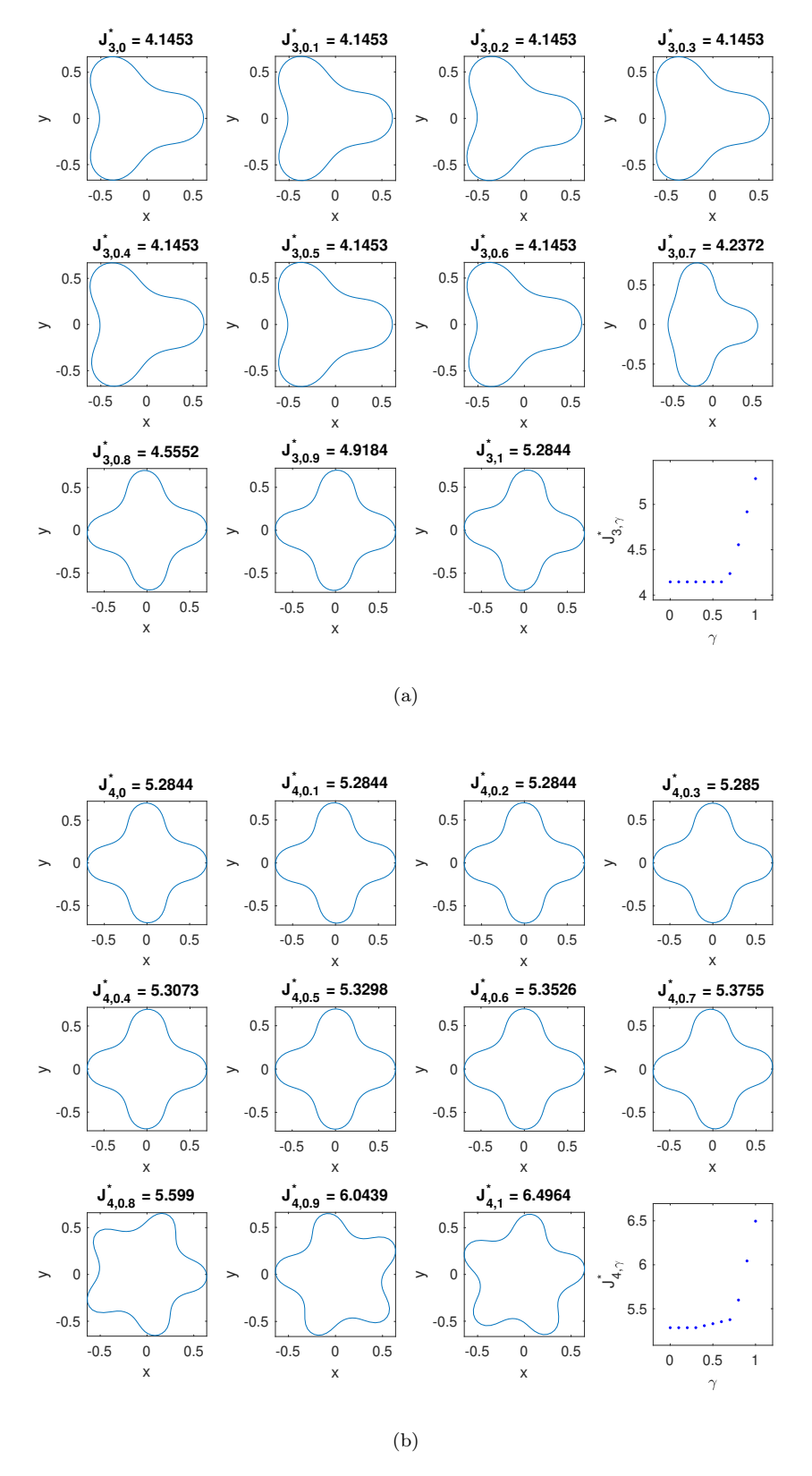


Figure 3.2: $J_{k,\gamma}^*$ for k=3,4 and $\gamma\in[0,1].$

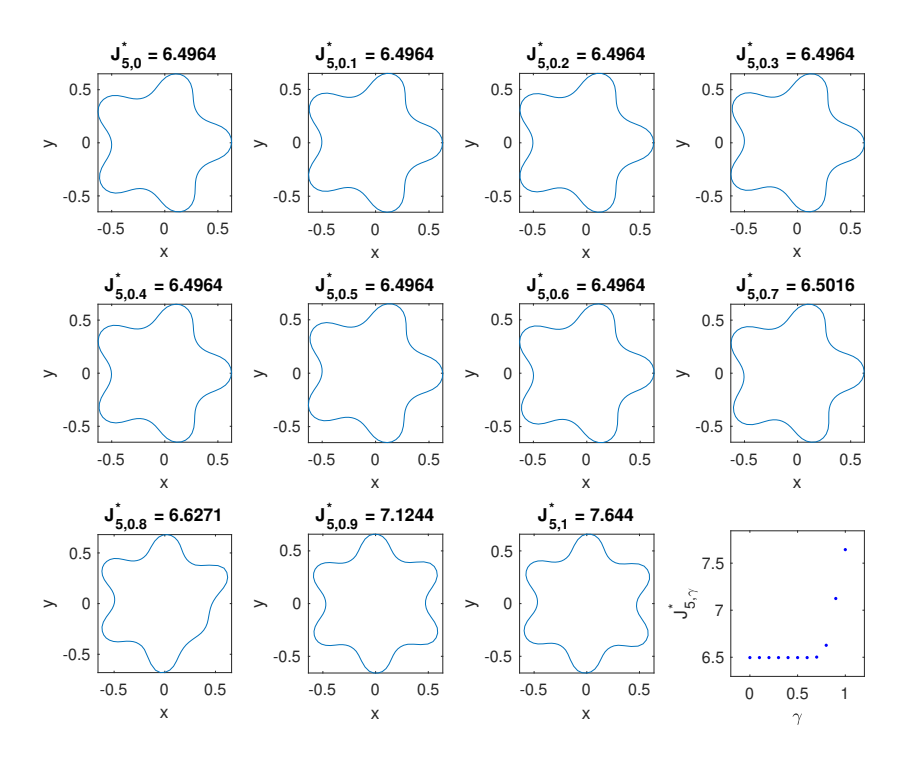


Figure 3.3: $J_{k,\gamma}^*$ for k = 5 and $\gamma \in [0,1]$.

4 The Range of the First Two Steklov Eigenvalues $(\lambda_1^A(\Omega), \lambda_2^A(\Omega))$

This section focuses on estimating the range of the first two Steklov eigenvalues $(\lambda_1^A(\Omega), \lambda_2^A(\Omega))$ for a simply-connected domain Ω . This range could be useful to obtain the bound of functions depending on λ_1^A and λ_2^A . The range of the first two Dirichlet-Laplacian eigenvalues $(\lambda_1^D(\Omega), \lambda_2^D(\Omega))$ was discussed in [32] and found to be bounded by two semi-infinite straight lines and a curve joining their end points. The curve can be determined by investigating the convex combination of the first two Laplacian eigenvalues. In order to find the range of the first two Steklov eigenvalues, we consider several one-parameter families of shapes including Cassini oval shapes and Hippopede shapes.

4.1 Cassini Oval Shapes

The Cassini oval shapes are generated by using the conformal mapping

$$f(w) = \alpha w \left(\frac{2}{1 + \alpha^2 - (1 - \alpha^2)w^2}\right)^{\frac{1}{2}}$$

that maps the unit circle to the Cassini oval. Here we show $(\lambda_1^A(\Omega_\alpha), \lambda_2^A(\Omega_\alpha))$ for $\alpha = 0.1:0.1:1$. When $\alpha = 1$, $f(\omega) = \omega$ which implies that the shape becomes a unit circle. The numerical estimation of eigenvalues were obtained by solving the Steklov eigenvalue problem (1.1) for each shape via spectral methods based on conformal mappings ([5]) instead of boundary integral methods [3] since the conformal

mapping is provided. We summarize the results in Table 6 and show the corresponding optimal shapes at each point $(\lambda_1^A(\Omega_\alpha), \lambda_2^A(\Omega_\alpha))$ in Figure 4.1(A).

$\lambda_k^A \setminus \alpha$	0.1	0.2	0.3	0.4	0.5	0.6	0.7	0.8	0.9	1
λ_1^A	0.3273	0.4864	0.6510	0.8216	0.9942	1.1648	1.3297	1.4867	1.6345	1.7725
λ_2^A	2.0850	2.3963	2.6889	2.8885	2.6739	2.4565	2.2551	2.0744	1.9141	1.7725

Table 6: $(\lambda_1^A(\Omega_\alpha), \lambda_2^A(\Omega_\alpha))$ of the Cassini oval shapes for different α .

4.2 Hippopede Shapes

We generate Hippopede shapes by using the mapping

$$f(w) = \frac{2\alpha w}{1 + \alpha + (1 - \alpha)w^2}$$

where $\alpha \in \{1/100, 1/16, 1/9, 1/4, 1/2, 3/4, 1\}$. This example was discussed in [18]. The Hippopede is a circle when $\alpha = 1$ while it approaches to two touching disks when $\alpha \to 0$. By using the same methods that were applied to Cassini oval shapes, the eigenvalues $(\lambda_1^A(\Omega_\alpha), \lambda_2^A(\Omega_\alpha))$ for the Hippopede shapes are shown in Table 7 and the corresponding optimal shapes are shown at each point $(\lambda_1^A(\Omega_\alpha), \lambda_2^A(\Omega_\alpha))$ in Figure 4.1(B).

$\lambda_k^A \setminus \alpha$	1/100	1/16	1/9	1/4	1/2	3/4	1
λ_1^A	0.4782	0.6988	0.8138	1.0490	1.3536	1.5866	1.7725
λ_2^A	2.5098	2.5307	2.5362	2.4720	2.2139	1.9646	1.7725

Table 7: $(\lambda_1^A(\Omega_\alpha), \lambda_2^A(\Omega_\alpha))$ of Hippopede shapes for different α .

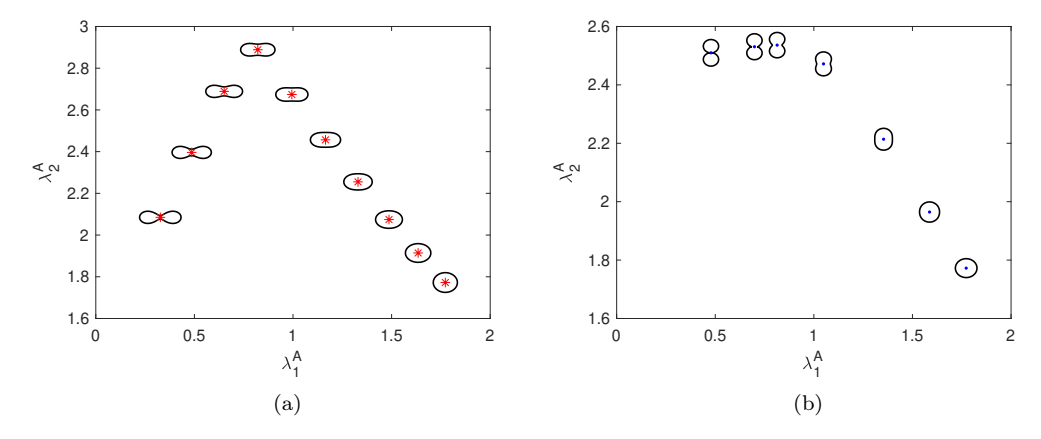


Figure 4.1: (A) $(\lambda_1^A(\Omega_\alpha), \lambda_2^A(\Omega_\alpha))$ for Cassini oval shapes . (B) $(\lambda_1^A(\Omega_\alpha), \lambda_2^A(\Omega_\alpha))$ for Hippopede shapes.

In Figure 4.2, in addition to the points we get from Cassini and Hippopede shapes, we plot the first two Steklov eigenvalues $(\lambda_1^A(\Omega), \lambda_2^A(\Omega))$ of the optimal shapes that maximized the k-th Steklov eigenvalue in the class of star-shaped domains [3, 5, 9]. This gives $\lambda_1^A \leq 1.7725$ which is achieved by a disk and $\lambda_2^A \leq 2.9161$ which is achieved by a two-fold symmetry shape. For the optimal shape that maximized the k-th Steklov eigenvalue, the first two eigenvalues are the same, i.e. $\lambda_2^A = \lambda_1^A$, for $k \geq 3$. It is observed that the Cassini oval and Hippopede shapes provide points in between upper bounds of λ_1^A and λ_2^A . Furthermore, we plot the

eigenvalues $(\lambda_1^A(R_a), \lambda_2^A(R_a))$ corresponding to the rectangular domain R_a that were found in section 2.1 and confirm numerically that the ratio of the first two eigenvalues $\lambda_2^A(R_a)/\lambda_1^A(R_a)$ of rectangles approach to 4 when $a \to 0$. We also observe that $\frac{\lambda_2^A}{\lambda_1^A} \approx 6.3703$ is achieved by Cassini oval shapes when $\alpha = 0.1$. Note that the shape that consists of two disjoint balls has $\lambda_0 = \lambda_1 = 0$, and $\lambda_2 = \sqrt{2\pi}$. Unlike the Dirichlet-Laplacian eigenvalue problem, the maximization of the ratio of the first two Steklov eigenvalue problems is not a well-posed problem.

In the beginning of this project, we thought that studying convex combination of first two Steklov eigenvalues will reveal precisely the range for the first two Steklov eigenvalues as people found out the range of the first two Dirichlet-Laplacian eigenvalues λ_k^D . It turns out that the optimizers shown in 3.1(A) are either a circle or a peanut shape which provides eigenvalues $(\lambda_1^A(\Omega), \lambda_2^A(\Omega))$ close to (1.7725, 17725) or (0.7771, 2.9161). We can only obtain numerical bounds which are given by $(1 - \gamma)\lambda_1^A(\Omega) + \gamma\lambda_2^A(\Omega) = J_{1,\gamma}^*$ without knowing all possible shapes that lie on the boundary of the range of $(\lambda_1^A(\Omega), \lambda_2^A(\Omega))$. See gray lines in Figure 4.2 and the numerical approximation of optimal shapes for max $J_{1,\gamma}$ which are indicated by green triangles. It would be interesting to determine the precise range of $(\lambda_1^A(\Omega), \lambda_2^A(\Omega))$ and the corresponding shapes that lie on the boundary of the range which will be pursued in future study.

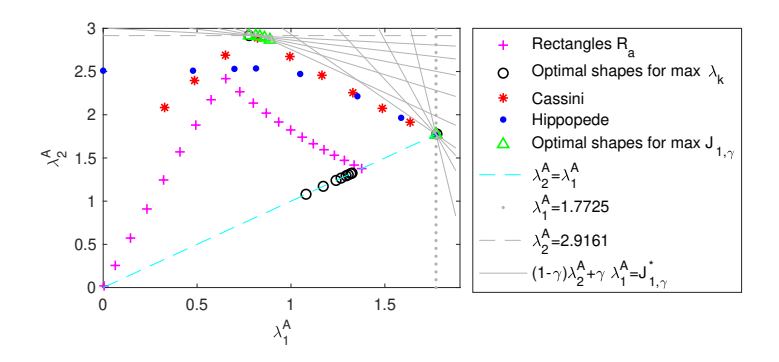


Figure 4.2: The range of the first two Steklov eigenvalues $(\lambda_1^A(\Omega), \lambda_2^A(\Omega))$ for several one-parameter families of shapes.

References

- [1] Hyun J Ahn. Vibrations of a pendulum consisting of a bob suspended from a wire: the method of integral equations. *Quarterly of Applied Mathematics*, 39(1):109–117, 1981.
- [2] Eldar Akhmetgaliyev. Fast numerical methods for mixed, singular Helmholtz boundary value problems and Laplace eigenvalue problems-with applications to antenna design, sloshing, electromagnetic scattering and spectral geometry. PhD thesis, California Institute of Technology, 2016.
- [3] Eldar Akhmetgaliyev, Chiu-Yen Kao, and Braxton Osting. Computational methods for extremal Steklov problems. SIAM Journal on Control and Optimization, 55(2):1226–1240, 2017.
- [4] Weaam Alhejaili. A numerical study of steklov eigenvalue problems. Claremont Graduate University, Ph.D. thesis, 2018.
- [5] Weaam Alhejaili and Chiu-Yen Kao. Numerical studies of the steklov eigenvalue problem via conformal mappings. *Applied Mathematics and Computation*, 347:785–802, 2019.
- [6] Giles Auchmuty and Manki Cho. Boundary integrals and approximations of harmonic functions. Numerical Functional Analysis and Optimization, 36(6):687–703, 2015.

- [7] Giles Auchmuty and Douglas R Simpkins. Spectral representations, and approximations, of divergence-free vector fields. *Quarterly of Applied Mathematics*, 74(3):429–441, 2016.
- [8] Rodrigo Banuelos, Tadeusz Kulczycki, Iosif Polterovich, and Bartlomiej Siudeja. Eigenvalue inequalities for mixed steklov problems. *Operator theory and its applications*, 231:19–34, 2010.
- [9] Beniamin Bogosel. The method of fundamental solutions applied to boundary eigenvalue problems. Journal of Computational and Applied Mathematics, 306:265–285, 2016.
- [10] Beniamin Bogosel, Doina Bucur, and Alessandro Giacomini. Optimal shapes maximizing the Steklov eigenvalues. SIAM Journal on Mathematical Analysis, 49(2):1645–1680, 2017.
- [11] Friedemann Brock. An isoperimetric inequality for eigenvalues of the stekloff problem. ZAMM-Journal of Applied Mathematics and Mechanics/Zeitschrift für Angewandte Mathematik und Mechanik: Applied Mathematics and Mechanics, 81(1):69–71, 2001.
- [12] Dorin Bucur and Ioan R Ionescu. Asymptotic analysis and scaling of friction parameters. Zeitschrift für angewandte Mathematik und Physik ZAMP, 57(6):1042–1056, 2006.
- [13] Pan Cheng, Jin Huang, and Zhu Wang. Nyström methods and extrapolation for solving Steklov eigensolutions and its application in elasticity. *Numerical Methods for Partial Differential Equations*, 28(6):2021–2040, 2012.
- [14] Marc Dambrine, Djalil Kateb, and Jimmy Lamboley. An extremal eigenvalue problem for the Wentzell–Laplace operator. In Annales de l'Institut Henri Poincare (C) Non Linear Analysis, 2014.
- [15] Bodo Dittmar. Sums of reciprocal Stekloff eigenvalues. Mathematische Nachrichten, 268(1):44-49, 2004.
- [16] Ailana Fraser and Richard Schoen. The first Steklov eigenvalue, conformal geometry, and minimal surfaces. Advances in Mathematics, 226(5):4011–4030, 2011.
- [17] Alexander Girouard and Iosif Polterovich. Spectral geometry of the Steklov problem. *J. Spectr. Theory*, 7(2):321–359, 2017.
- [18] Alexandre Girouard, Richard S Laugesen, and BA Siudeja. Steklov eigenvalues and quasiconformal maps of simply connected planar domains. *Archive for Rational Mechanics and Analysis*, 219(2):903–936, 2016.
- [19] Alexandre Girouard, Richard S. Laugesen, and Barthomiej A. Siudeja. Steklov eigenvalues and quasiconformal maps of simply connected planar domains. Archive for Rational Mechanics and Analysis, 2015.
- [20] Alexandre Girouard and Iosif Polterovich. On the Hersch-Payne-Schiffer inequalities for Steklov eigenvalues. Functional Analysis and its Applications, 44(2):106–117, 2010.
- [21] Frédéric Hecht. New development in freefem++. Journal of numerical mathematics, 20(3-4):251–266, 2012.
- [22] Antoine Henrot, Gérard A Philippin, and A Safoui. Some isoperimetric inequalities with application to the stekloff problem. *Journal of Convex Analysis*, 15(3):581–592, 2008.
- [23] Joseph Hersch, Lawrence E Payne, and Menahem M Schiffer. Some inequalities for Stekloff eigenvalues. Archive for Rational Mechanics and Analysis, 57(2):99–114, 1974.
- [24] Raouf A Ibrahim. Liquid sloshing dynamics: theory and applications. Cambridge University Press, 2005.
- [25] Mette Iversen and Dario Mazzoleni. Minimising convex combinations of low eigenvalues. ESAIM: Control, Optimisation and Calculus of Variations, 20(2):442–459, 2014.

- [26] Vladimir Kozlov and Nikolay Kuznetsov. The ice-fishing problem: the fundamental sloshing frequency versus geometry of holes. *Mathematical methods in the applied sciences*, 27(3):289–312, 2004.
- [27] Michael Levitin, Leonid Parnovski, Iosif Polterovich, and David A Sher. Sloshing, Steklov and corners i: Asymptotics of sloshing eigenvalues. arXiv preprint arXiv:1709.01891, 2017.
- [28] Braxton Osting and Chiu-Yen Kao. Minimal convex combinations of sequential laplace–dirichlet eigenvalues. SIAM Journal on Scientific Computing, 35(3):B731–B750, 2013.
- [29] Braxton Osting and Chiu-Yen Kao. Minimal convex combinations of three sequential laplace-dirichlet eigenvalues. Applied Mathematics & Optimization, 69(1):123–139, 2014.
- [30] B Andreas Troesch. An isoperimetric sloshing problem. Communications on Pure and Applied Mathematics, 18(1-2):319–338, 1965.
- [31] Robert Weinstock. Inequalities for a classical eigenvalue problem. *Journal of Rational Mechanics and Analysis*, 3(6):745–753, 1954.
- [32] Sven Andreas Wolf and Joseph B Keller. Range of the first two eigenvalues of the laplacian. *Proc. R. Soc. Lond. A*, 447(1930):397–412, 1994.